

Diffuse HI Disks in Isolated Galaxies

David E. Hogg¹, Morton S. Roberts¹, Martha P. Haynes,^{2,3} Ronald J. Maddalena⁴

ABSTRACT

In order to investigate the contribution of diffuse components to their total HI emission, we have obtained high precision HI line flux densities with the 100 m Green Bank Telescope for a sample of 100 isolated spiral and irregular galaxies which we have previously observed with the 43 m telescope. A comparison of the observed HI line fluxes obtained with the two different telescopes, characterized by half-power beam widths of 9' and 21' respectively, exploits a “beam matching” technique to yield a statistical determination of the occurrence of diffuse HI components in their disks. A simple model of the HI distribution within a galaxy well describes $\sim 75\%$ of the sample and accounts for all of the HI line flux density. The remaining galaxies are approximately evenly divided into two categories: ones which appear to possess a significantly more extensive HI distribution than the model predicts, and ones for which the HI distribution is more centrally concentrated than predicted. Examples of both extremes can be found in the literature but little attention has been paid to the centrally concentrated HI systems. Our sample has demonstrated that galaxies do not commonly possess extended regions of low surface brightness HI gas which is not accounted for by our current understanding of the structure of HI disks. Eight HI-rich companions to the target objects are identified, and a set of extragalactic HI line flux density calibrators is presented.

Subject headings: galaxies: spiral; — radio lines: galaxies

1. Introduction

In most gas-rich galaxies, the HI component consists of a disk which exhibits well-ordered circular motions and maintains its dynamical structure well outside the optical disk. Truncation

¹National Radio Astronomy Observatory, 520 Edgemont Road, Charlottesville, VA 22903. The National Radio Astronomy Observatory is operated by Associated Universities, Inc. under a cooperative agreement with the National Science Foundation. *e-mail:* dhogg@nrao.edu, mroberts@nrao.edu

²Center for Radiophysics and Space Research, Space Sciences Building, Cornell University, Ithaca, NY 14853. *e-mail:* haynes@astro.cornell.edu

³National Astronomy and Ionosphere Center, Cornell University, Space Sciences Building, Ithaca, NY 14853. The National Astronomy and Ionosphere Center is operated by Cornell University under a cooperative agreement with the National Science Foundation.

⁴National Radio Astronomy Observatory, P.O. Box 2, Green Bank, WV 24944. *e-mail:* rmaddalena@nrao.edu

of the stellar disk at 3 – 5 optical disk scale lengths is suggested by models based on gas density thresholds (Fall & Efstathiou 1980) and by those related to the maximum protogalaxy specific angular momentum (van der Kruit 1979). On the other hand, a very extended HI disk may represent a reservoir for future star formation activity. For a sample of 108 galaxies mapped with the Westerbork Synthesis Radio Telescope (WSRT), Broeils & Rhee (1997) found the ratio of HI to optical radius, $R_{HI}/R_{25} \sim 1.7 \pm 0.5$. Extreme examples with $R_{HI}/R_{25} \sim 5$ are also known, such as DDO 154 (Krumm & Burstein 1984), NGC 4449 (Bajaja *et al* 1994), NGC 2915 (Meurer *et al* 1996) and NGC 3741 (Begum, Chengalur & Karachentsev 2005). Such extensive HI serves as a powerful tool for evaluating the dark matter in a galaxy. For example, the HI rotation curve in NGC 3741 (Gentile *et al* 2007) can be traced to 42 B-band disk scale lengths. Thus, the kinematics can be measured and evaluated in a region where there is essentially no optical light, resulting in a very large mass-to-light ratio. Although the causal reason is unknown, the dark matter distribution in disk galaxies appears to mimic closely that of the HI.

This low density outer gas also bears on the star formation and evolutionary history of the galaxy. It may represent the reservoir that feeds star formation (Larson, Tinsley & Caldwell 1980). Stochastic star formation in low density regions could produce with time an extremely low surface brightness stellar halo, perhaps with an IMF biased towards low masses. Gas may also be accreted in minor merger events; depending on the encounter configuration, the accreted gas could spread into an extended disk (Quinn, Hernquist & Fullagar 1993). The existence of such diffuse disks may complicate both the derivation of HI masses, for which flux may be missed by insufficient spatial sampling, and the understanding of the cross section for damped Lyman α absorption in the nearby universe. We note the importance of low surface brightness extended stellar disks in the low surface brightness galaxies such as Malin I; how often do similarly extended components exist in the HI distribution of spiral disks?

Most studies of the gas distribution in galaxies employ aperture synthesis imaging techniques. However, single dish observations can provide unique and complementary information on the large scale low density gas. The spatial resolution advantages of array imaging are obvious. The major disadvantage of interferometers, however, is that the gas distribution on the largest spatial scales may be resolved out because of the absence of the so-called “zero spacing” Fourier components. In such circumstances, large beams, contributed by single dish instruments, will detect the total HI flux density, including the low density, large scale diffuse gas. Comparison of total HI line flux density measurements obtained with a variety of single dish telescopes, delivering a range of beam sizes, can provide a sensitive measure of extended diffuse components. The fraction of the total flux density emitted by the galaxy which is intercepted by the antenna beam is a function of the brightness distribution of the emission convolved with the antenna beam (Shostak & Allen 1980; Hewitt, Haynes & Giovanelli 1983: HHG). “Beam-matching” experiments, which compare the HI line flux densities detected by telescopes with significantly different beam sizes, probe the large-spatial scale source structure by exploiting the changing beam-filling factor. As the source-to-beam ratio increases, the detected HI line flux density will decrease. Thus, beam matching

experiments can provide an efficient method of estimating the fraction of HI gas in the most diffuse and extended components without requiring extensive mapping (Hunter & Gallagher 1985; Du Prie & Schneider 1996).

The principle drawback to the beam-matching method is the requirement of adequate accuracy in the flux density measurements from the telescopes of different sizes. As demonstrated by van Zee *et al* (1997), it is possible to obtain flux calibration of HI line spectra accurate to better than 5% using frequent monitoring of absolute flux calibrators. The development by van Zee *et al* of an observing methodology which is capable of producing very accurate line flux densities offers the potential for the application of a single dish “beam matching” technique to explore statistically the occurrence of very diffuse HI components using two telescopes with significantly different beam solid angles.

In an earlier study (Haynes *et al* 1998; hereafter, Paper I) we reported observations of accurately calibrated HI line emission profiles of 104 relatively isolated spiral and irregular galaxies which were obtained using the 43 m telescope of the NRAO at Green Bank. Those data were used to discuss asymmetries in the global HI profiles of normal galaxies, but we also intended to use these observations as the first step in a program to search for faint, extended HI emission. The current work presents the culmination of the program, exploiting newly obtained HI line profiles for a significant subset of the same galaxies observed, in this instance, with the 100 m Green Bank Telescope (GBT).

Our decision to use the GBT in the second epoch of the program was based on two considerations. First, the solid angle of the beam of the GBT is approximately five times smaller than that of the 43 m telescope, so that many of the objects which were unresolved or slightly resolved in the first series of observations will be well resolved with the GBT. Second, because the GBT has an unblocked aperture, it was expected that the effects of interference, standing waves, and baseline ripples would be much reduced, so that features introduced by the telescope would be correspondingly less important. This paper reports the results of this 43 m telescope – GBT beam-matching experiment.

We present the new GBT observations in Section 2. The method employed to infer the HI extent from comparison of the HI line flux densities observed with each of the two telescopes and the results of that analysis is presented in Section 3. Section 4 presents our conclusions. A Hubble constant of $70 \text{ km s}^{-1} \text{ Mpc}^{-1}$, combined with a Virgo-centric infall flow model (Tonry *et al* 2000; Masters 2005), is used for distance dependent calculations, unless otherwise specified.

2. Observations

The observations reported here were conducted during the early commissioning phase of the GBT. The observing list included the majority of galaxies whose HI line profiles were presented in Paper I and therefore are characterized by the selection criteria discussed therein: targets have a

known HI line flux density $\int SdV$ greater than 10 Jy km s^{-1} , heliocentric velocity $< 3000 \text{ km s}^{-1}$, Galactic latitude $|b| > 20^\circ$, and Declination $> -20^\circ$. Furthermore, objects were chosen to have no known (at the time) companions within a projected separation of less than 0.5° and with a velocity difference of less than 400 km s^{-1} . An additional sensitivity criterion was imposed by selecting only those objects for which the ratio of the HI line flux integral $\int SdV$ to the observed HI line velocity width W is greater than 0.02. Some attempt was made to include gas rich objects over a broad range of morphological types. 100 of the 104 galaxies discussed in Paper I were observed with the GBT.

Because of the requirement to make precision observations, the list of galaxies observed in Paper I was divided into two parts, so that the measurements could be conducted primarily at night. Objects in the range of Right Ascension from 14–8 hours were observed in the period August 1–4, 2002. Those in the range 3–17 hours were observed between February 9 and March 4, 2003. Difficulties in completing the survey forced some of the observations to be made in the early morning. In addition, some of the observations made during the second epoch suffered from bad weather and were impossible to calibrate accurately. In order to complete the survey and to establish the calibration of all of the observations, we requested an additional observing time allocation which was scheduled on January 17 and January 21, 2005.

Since the GBT Spectrometer was not routinely available at the time of the first observations in 2002, we used the Spectral Processor as the backend during the first epoch. For consistency, we also used it in the subsequent epochs. This FFT spectrometer supports 1024 channels on each of the two receiver IF's and is capable of bandwidths up to 40 MHz. For our application we used bandwidths of either 5 MHz or 10 MHz, yielding a channel width of 1 km s^{-1} or 2 km s^{-1} respectively.

The observational technique employed was similar to that used for the 43 m telescope observations reported in Paper I. The pointing of the GBT is very stable, so that checks of the pointing offsets were only needed at intervals of one to two hours. The observations of the galaxies used the total-power beam-switching mode as a sequence of off-source and on-source pairs lasting approximately ten minutes. The off-source position was displaced in Right Ascension by 6 minutes, so that the telescope tracked the same range of hour angle as covered during the on-source observation. The total integration time differed from source to source, depending on the source line flux density observed in the earlier observation with the 43 m telescope, and ranged between ten minutes and 60 minutes.

2.1. Calibration

At the outset it was intended that the calibration of the GBT observations would proceed in the same manner as was employed previously with the 43 m. Observations of the galaxies were interspersed with observations of quasars and radio galaxies in order to tie the flux scale directly to that of Ott *et al* (1994). However, the IF system during the earliest period of operations had

only a narrow range of input power level for which it was linear. As a consequence, the system gain established by observations of strong calibrators whose flux essentially doubled the system temperature was not correct when applied to much weaker sources.

In the course of the third epoch of observations, we observed a dozen continuum sources having fluxes which ranged between approximately 20 Jy (typical of the Ott sources) and 1 Jy. We then fitted a second-order gain expression of the form:

$$P_{out} = AP_{inp} + B(P_{inp})^2 \quad (1)$$

where P_{out} is the observed output power level produced by an input power level P_{inp} ,

$$P_{inp} = P_{sou} + P_{sys} \quad (2)$$

P_{sou} is the power contributed by the radio source, and P_{sys} is the sum of the contributions from the atmosphere, ground, and receiver.

By firing the receiver’s calibration noise diode while pointing towards a continuum calibration source and then again on blank sky, one obtains four equations of the form of Equation 1, that is, equations for all four combinations of ON source and OFF source, diode ON, and diode OFF. From this system of simultaneous equations, and using the P_{sou} from the Ott *et al* catalog, one can determine A, B, P_{sys} and the intensity of the noise diode, T_{cal} . Since the backend used for these measurements is the same as that used for the HI observations, the coefficients and T_{cal} values can be applied to the HI observations. We then estimated that the effect of the 2nd order gain correction would not alter the calibration by more than 1%, an amount which is smaller than our other systematic effects, so we dismissed the need to perform a non-linear correction.

In transferring the calibration from the third epoch to the first two epochs, care was taken in the selection of the galaxies such that at least one secondary had been observed in each day of the earlier epochs, and in most cases there were more than one of these secondary profile calibrators.

The bandpass of each of the receiver IF’s is a smooth function of frequency which varies by between 2% and 3% in the frequency range 1405 – 1420 MHz, depending on the IF and the epoch. Gain terms were computed from the continuum calibrator at intervals of 1 MHz, providing corrections which were within 0.1%.

The observations from the third epoch provided us with a suite of gain terms derived from both the continuum calibrators and from the integrated profiles of a number of galaxies defined to be secondary calibrators. We found that this combination of the continuum sources and secondary profile calibrators gave consistent gain terms for the first epoch, though the results for the first IF channel, corresponding to one polarization sense (“XX”), showed more scatter. However, the scheduling in the second epoch involved many more days, each of which had only a few hours of observations. Because of this, the analysis of the continuum sources did not provide sufficient gain

information to calibrate the data base. In addition, the first IF channel proved to be completely unreliable during the second epoch and had to be abandoned. The gain terms for the second IF channel, recording the orthogonal polarization (“YY”), were derived entirely from the secondary calibrators. Even with this special treatment, it was not possible to salvage all of the data, and hence four of the galaxies in Paper I were not measured with the GBT.

The integrated HI flux density for each galaxy was obtained from the calibrated profile using a reduction technique similar to that employed in Paper I. Briefly, the baseline level was defined using signal-free channels on either side of the profile. The area under the profile was measured relative to the baseline, using as integration limits the velocity channels on each side at which the intensity first exceeded the rms noise per channel. As noted in Paper I, this definition of the line flux density is intended to include the flux density contained in the profile wings, and therefore to ensure that the GBT results can be compared with those from the 43 m. The HI line flux integrals are given in Table 1.

For a source of line flux integral of 50 Jy km s^{-1} , having a profile width of 200 km s^{-1} , and observed with an rms noise per 2 km s^{-1} channel of 10 mJy , the uncertainty in the line flux integral due to the noise alone is less than 0.6%. A greater error arises from the fitting of the polynomial baseline, and in the definition of the velocity range over which the integration is made. In the case of the GBT, the unblocked aperture contributes to stable and typically linear baselines, both because the standing waves characteristic of blocked apertures are absent, and because the amount of stray radiation is reduced. In more than 80% of the spectra, the baseline could be well-modeled by a linear slope. In fewer than 3% of the observations was it necessary to fit a baseline of higher order than three. We estimate that the error in the measured line flux integrals is less than 2% for galaxies having line flux integrals greater than 20 Jy km s^{-1} .

The line flux integrals have been corrected for atmospheric extinction, and are on the flux density scale of Ott *et al* (1994). They therefore are directly comparable with the line flux integrals from Paper I. However, we emphasize that the line flux integrals from the GBT must not be used as an estimate of the total HI flux densities since in almost all cases the galaxies have been resolved with the GBT.

Table 1 summarizes the GBT observations, and compares them with the 43 m results from Paper I. Columns are as follows:

Column 1: Entry number in the Uppsala General Catalog (UGC; Nilson 1973) or in the private galaxy database of M.P.H. and R. Giovanelli known as the Arecibo General Catalog (AGC).

Column 2: Alternate name, including the NGC or IC name, or other common names including the entry designation in the *Catalog of Galaxies and Clusters of Galaxies* (Zwicky *et al* 1960-68) or the *Morphological Catalog of Galaxies* (Vorontsov-Velyaminov & Arhipova 1968). Note that the entry names for the latter catalog are compressed to 8 digits.

Column 3: The R.A. and Dec. in (J2000) coordinates.

Column 4: The major axis and minor axis diameters, $D_{25} \times d_{25}$, measured in the blue, from the *Third Reference Catalog of Galaxies* (de Vaucouleurs *et al* 1991: RC3), in arcmin.

Column 5: The morphological type code index, T, from the RC3.

Column 6: The heliocentric systemic velocity, V_{21} , taken as the midpoint of the profile at the 50% level, in km s^{-1} .

Column 7: The adopted distance, in Mpc, calculated from V_{21} using the local flow field model of Tonry *et al* (2000) or as given by primary distance methods in the compilation of Masters (2005).

Column 8: The full velocity width of the HI profile measured at a level of 50% of the peak, in km s^{-1} .

Column 9: The integrated HI line flux density measured with the 43 m telescope, as reported in Paper I, S_{43m}^{obs} , in Jy-km s^{-1} .

Column 10: The integrated HI line flux density measured with the GBT (this work), S_{GBT}^{obs} , in Jy-km s^{-1} .

Column 11: The resolution of the GBT spectrum, δV , in km s^{-1} , after Hanning smoothing.

Column 12: The rms noise per channel of the GBT spectrum, in mJy.

For comparison, we note that the observations of Paper 1 were made with a channel separation of either 1 or 2 km s^{-1} . Total on-source integration times of 1-2 hr yielded values of the noise per channel of ~ 10 mJy. The largest source of uncertainty in the determination of the flux density is again the baseline determination, where we estimated the effect to be approximately 3 %.

3. Comparison of the 43 m and GBT Results

Given the three to five percent accuracy of the integrated HI line flux densities measured with the two telescopes as presented in Table 1, we expect $S_{43m}^{obs} > S_{GBT}^{obs}$ for those objects which are partially resolved by the GBT beam.

As expected, the flux integrals which are measured with the GBT are usually either equal to or less than the corresponding values measured with the 43 m which were reported in Paper I. Figure 1 shows a sample of the GBT profiles superimposed upon the profiles from the 43 m telescope. The comparison plots for all of the objects in the sample are available electronically. For galaxies which are small in angular extent, such as the case for UGC 9328 (top panel), the agreement between the profiles is good, even when the profile is significantly lopsided. In this instance, the asymmetry must result from a real asymmetry in the HI distribution. In some instances, as exemplified by UGC 231 (middle panel), the outer parts of the HI distribution have been resolved by the GBT with a consequent reduction in the amplitude of the horns in the profile. If the galaxy is more heavily resolved, there is a reduction in the amplitude across the entire profile, as illustrated by

the profile of UGC 9436 (lower panel).

To begin the analysis of the HI flux integrals measured with the GBT, we show in Figure 2 the distribution of the ratio of the measured 43 m flux integral to the measured GBT flux integral for each of the 100 galaxies contained in Table 1. The observed flux ratio $FR^{obs} = S_{43m}^{obs}/S_{GBT}^{obs}$ peaks at a value of approximately 1.05. This flux ratio is that expected for a galaxy viewed face-on having a Gaussian HI disk of diameter (FWHM) $2.2'$. Forty percent of the objects are seen to have a GBT flux lower by ten percent or more compared to the 43 m flux, indicating that the diameter (FWHM) of the HI distribution exceeds $3.2'$, if the galaxy had a Gaussian disk and was viewed face-on.

The dispersion in the observed ratios is a combination of the observational errors and the variations in the ratio arising from the differences in the distribution of the HI in the galaxies. We can estimate the approximate contribution of the measurement errors by noting that there are eleven galaxies which have an observed flux ratio less than 1.0. Since the minimum ratio that can be realized physically is 1.0, these values must reflect the measurement errors. The distribution of flux ratios between 0.9 and 1.03 can be approximated by a half-Gaussian of standard deviation 0.035. In Paper I, it was estimated that the uncertainty in an individual line flux is 3%, excluding uncertainties in the flux scale, and is dominated by the uncertainty in the spectral baseline. The dispersion in Figure 2 implies that the error contribution arising from the GBT data is smaller than that from the 43 m, consistent with the estimated error above.

The observed ratio FR^{obs} does not enable a unique estimate of the factors by which the observed fluxes must be increased to more accurately estimate the total HI flux from the galaxy, since details of the HI distribution (e.g., form of the radial distribution, presence of spiral arms, holes, etc) govern the effectiveness with which each antenna beam samples the total HI content in the galaxy. In most well-behaved HI disks, the azimuthally-averaged HI distribution can be described by a Gaussian or exponential function (Shostak 1978; HHG; Broeils & Rhee 1997; Swaters *et al* 2002). In dwarfs, it is often peaked toward the center, while in spirals, the HI layer often shows a central depression, especially in the bulge-dominated region. To judge the amount by which the galaxies have been resolved, we adopt the model for the HI distribution described by HHG, which is a scaled version of the double Gaussian model of Shostak (1978). HHG assumed that the HI surface density σ_H could be described by the sum of two Gaussian components

$$\sigma_H = 3exp(-r^2/R_o^2) - 1.8exp[-r^2/0.23R_o^2] \quad (3)$$

where R_o was found to be 25 kpc (see their Equation 3).

In this model, the larger (positive amplitude) component represents the extended HI disk while the smaller component (negative amplitude) accounts for the commonly-present central depression. In the absence of spatially resolved information on the HI distribution, its angular scale and axial ratio are assumed to be related to those given by the stellar distribution by a simple scaling factor. Under such assumptions, the fraction of the source's HI line emission which is detected by a given

telescope’s beam is given by

$$f = \frac{\sum_{j=1,2} \left[\frac{a_j \theta_j^2}{(1+\theta_j^2/\theta_B^2)^{1/2} (1+\theta_j^2 \cos^2 i / \theta_B^2)^{1/2}} \right]}{\sum_{j=1,2} a_j \theta_j^2} \quad (4)$$

Following HHG, we adopt a projected double Gaussian HI distribution σ_H of amplitude $a_2 = -0.6a_1$ and relative extent $\theta_2 = 0.23\theta_1$. It should be noted that the characteristic beam extent θ_B in the above equation is not the usually-quoted half power beam width, but is rather the angular extent at which the adopted Gaussian beam power pattern falls to e^{-1} of its central value. The “beam coupling factor” f^{BC} by which the observed HI line flux density must be corrected to yield a value corrected for source extent is the inverse of this fraction, that is, the HI line flux density corrected for beam dilution $S^{corr} = S^{obs} \times f^{BC}$.

By convolving the assumed HI distribution with the antenna beams of the two telescopes, we can predict what flux ratio should have been measured. Note that HHG used the UGC diameter; we use the scaling relations derived in the RC3 to convert D_{25} to D_{UGC} , and like HHG assume that the “characteristic” HI diameter D_{HI} is 1.1 D_{UGC} , so that $\theta_1 = 0.55 R_{UGC}$. The inclination is derived from the observed RC3 axial ratio assuming an intrinsic axial ratio of 0.17 for galaxies of type Sc and 0.20 for all other types. Once the beam coupling factor and thus the beam-corrected HI line flux density is computed for each telescope, we can predict the “expected” HI line flux ratio $FR^{exp} = S_{43m}^{corr}/S_{GBT}^{corr}$.

Figure 3 compares the observed HI line flux ratios to the predicted flux ratios for the galaxies. Two galaxies, UGC 5079 and UGC 7524, have been omitted because the estimated correction factor exceeds 1.5 in each case, and is therefore likely to be much more uncertain than the corrections for the galaxies of smaller angular scale. The subsequent discussion will concentrate on the remaining 98 objects.

There is correlation between the observed and predicted flux ratios, at a significance of 99%, but there is considerable scatter in the points. Some of the scatter is introduced by the uncertainty in the measured flux ratio. Using 3% as the uncertainty in the 43 m flux densities of the brighter galaxies, and the uncertainty of 2% in the GBT flux density for such sources we expect that the observational uncertainty in the ratio would be approximately 3.5%. Larger deviations must arise because of the failure of the model to represent the distribution of HI in the galaxies. The dashed lines in Figure 3 isolate galaxies for which the predicted ratio differs from the observed ratio by more than 10%, or three sigma; deviations of this size are not expected to arise from observational error. We will examine these deviations in more detail by defining a flux ratio index:

$$FluxRatioIndex = [FR^{exp} - FR^{obs}]/FR^{exp} \quad (5)$$

where FR^{exp} is the ratio of flux at the 43 m to that at the GBT expected on the basis of the

model, and FR^{obs} is the corresponding ratio as observed. In this definition, the Flux Ratio Index is zero for any galaxy in which the HI distribution is approximately that posited in the model. It is less than zero if the flux observed with the GBT is less than expected, since then the observed ratio will be large. This situation arises if the actual HI distribution is more extensive than that assumed in the model HI distribution, that is, the gradient of the gas is more gradual than that in the model described by equation 3. In contrast, the Flux Ratio Index is greater than zero if the observed ratio is unexpectedly small, and indicates that the actual HI distribution is more centrally condensed than in the model.

As can be seen in Figure 3, the majority of the sample, $\sim 75\%$, satisfy the simple model of the HI distribution described in equation 3. The remaining systems are divided approximately evenly between those with a more extensive and those with a more compact distribution than that of the model.

In principle, additional constraints on the HI distribution for many of the galaxies can be obtained from the fluxes measured in the HIPASS survey made with the Parkes telescope, since its beam is intermediate between those of the 43 m and the GBT. However, because the HIPASS survey was not intended to be a photometric survey, its flux densities do not reach the level of accuracy required for our purposes.

3.1. Galaxies with an extensive HI distribution

The GBT observations for twelve galaxies show that their flux ratio index is less than -0.1, that is, the HI disk is more extensive than predicted by the model. The properties of these galaxies are summarized in Table 2 in which the entries are as follows:

- Column 1: The galaxy identifying number, as in Table 1.
- Column 2: The morphological type code index, T, from the RC3.
- Column 3: The Flux Ratio Index as defined by equation 5.
- Column 4: The diameter measured in the blue from the RC3, D_{25} , in kpc.
- Column 5: The diameter of the HI envelope, D_{HI} , in kpc. References to the published maps are noted.
- Column 6: The ratio of the HI and optical diameters, D_{25}/D_{HI} .
- Column 7: The logarithm of the HI mass, M_{HI} , in solar masses.
- Column 8: The logarithm of the blue luminosity, L_B , in solar luminosities, based on the blue magnitude from the RC3. The adopted value of the solar blue absolute magnitude is +5.48.
- Column 9: The logarithm of the ratio of the HI mass to the blue luminosity M_{HI}/L_B .

Four of the galaxies in Table 2 have published HI maps which can be used to estimate an HI diameter. For all but UGC 1736, the values of the diameters are for a surface density of $1 M_{\odot}/\text{pc}^2$, and have been taken directly from the reference. The diameter of UGC 1736 was estimated from the map of Espada *et al* (2005) by D.E.H., corresponding to an HI surface density of $\sim 4 M_{\odot}/\text{pc}^2$. The observed HI diameters for three of the galaxies are greater than D_{25} by a factor of two or more, whereas the typical ratio is 1.7 (c.f. Broeils & Rhee 1997), and thus these objects are indeed more extended than would be expected. That approximately 10% of the sample have relatively large diameters is consistent with surveys made with mapping instruments. For example, Swaters *et al* (2002) found 22% of a sample of 73 late-type dwarf galaxies had the ratio of HI diameter to D_{25} greater than 2.3. Broeils & Rhee found that 10% of the spiral and irregular galaxies in their sample of 108 galaxies had ratios greater than 2.3.

With a ratio of 1.7, UGC 6817 stands in marked contrast to the other three. It is included in the list of extensive objects because the GBT observed a smaller flux than expected. The model assumed the optical inclination of 69 degrees, based on the RC3 measurements. However, the HI map of Swaters *et al* (2002) shows that the HI is quite extended in the direction of the minor axis. The axial ratio at a surface density of $1 M_{\odot}/\text{pc}^2$ is 0.7, approximately twice the optical value. The amount by which the GBT resolves the source is therefore much greater than expected using a model based on the optical properties.

It is not surprising to find that 40% (5/12) of the systems we identify as having extensive HI envelopes also have HI rich companions (Table 4). Clearly the model distribution fails when the HI distribution extends well beyond that expected.

3.2. Galaxies with a concentrated HI Distribution

The GBT observations for ten galaxies show their flux ratio index is greater than 0.1, that is, the HI disk is more concentrated than predicted by the model. The properties of these galaxies are summarized in Table 3. The columns are as described for Table 2. D.E.H. estimated the diameter for UGC 3574 from the map in the WHISP survey, and for UGC 7698 from the map of Stil & Israel (2002). The diameters are measured at a surface density of $1 M_{\odot}/\text{pc}^2$.

Two of the galaxies, UGC 4325 and UGC 11670, were observed to have a larger flux integral with the GBT than with the 43 m. As noted above, this must reflect the influence of observational error, and the flux ratio index must be an upper limit.

The observed HI diameters of the ten galaxies are all less than the 1.6 times the RC3 diameter, and six have a ratio smaller than 1.4. This is somewhat fewer than would be expected on the basis of the survey of Broeils & Rhee (1997), who found that 23% of the spirals and irregulars which they mapped had a ratio less than 1.4. For smaller objects where the predicted ratio is close to one the noise in the measurement will be of relatively greater importance in the test of whether the flux ratio index lies near zero, and it is possible therefore that we have underestimated the fraction

of galaxies which are compact. Special note should be made of UGC 7698, since neither Broeils & Rhee nor Swaters *et al* (200) had any galaxies for which the HI diameter was smaller than the RC3 optical size.

3.3. Galaxy Companions

The original sample was chosen to be isolated on the basis of a catalog (AGC) with redshifts complete to $m \sim 15.4$ and/or diameter greater than $1'$. The detection of HI-rich companions fainter or smaller than these limits was expected because of the relatively large beam, $21'$, and high sensitivity employed in the Paper I observations. Comparison with profiles obtained with the GBT $9'$ beam is an aid in identifying such companions especially when their velocity profiles blend with that of the target galaxy. Eight likely detections are given in Table 4 which is divided into two sections: (1) the target galaxy and (2) its likely companion. The entries in this table are as follows:

For the target galaxy:

Column 1: Galaxy identifying number, as in Table 1.

Column 2: Alternate name, as in Table 1.

Column 3: Heliocentric radial velocity, V_{21} , in km s^{-1} .

For each companion galaxy:

Column 4: Galaxy identifying number, as in Table 1.

Column 5: Alternate name, as in Table 1.

Column 6: Position of companion, in J2000 coordinates, as given in NED.

Column 7: Heliocentric radial velocity, V_{dot} , in km s^{-1} , from NED.

Column 8: Angular separation of the companion from the target galaxy, θ , in arcmin.

Column 9: Apparent magnitude, m_B , from NED.

Column 10: Estimate of angular diameter, D_{25} , in arcmin.

Column 11: Morphological type index, T, in the RC3 system, from NED or estimated by us.

The HI velocity profiles of the target galaxies obtained with the 43 m and the GBT are shown in Figure 4. These eight galaxies represent a lower limit to the number of nearby companions. Three additional galaxies, each with a previously recognized nearby companion, were intentionally included in our initial sample (see Paper I): NGC 5324, NGC 7468, and IZw 18. These are not included in our statistics of serendipitously discovered companions.

The most obvious marking of a companion is an additional profile well separated in velocity

from that of the target galaxy profile, e.g. UGC 2141 (NGC 1012). In that case, the HI profile observed with the 43 m telescope includes a contribution from the small irregular object dubbed AGC 122790 10.4' from the main target. This small dwarf, noted first by Vennik & Richter (1993) has been detected by the WSRT survey of Braun, Thilker & Walterbos (2003) at $V_{\odot} = 810 \text{ km s}^{-1}$.

As the velocity difference between target and companion galaxy decreases the two profiles blend resulting in an asymmetrical profile. Examples of partial profile merging include UGC 3384 and UGC 3647 (see Figure 4).

3.4. Extragalactic HI Calibrators

The dual beam observations reported here allow us to identify a number of galaxies well-suited to serve as HI calibrators. These galaxies, listed in Table 5 and whose HI line profiles are illustrated in Figure 5, have small beam coupling corrections for the 43 m ($\leq 2\%$). They are validated by the narrower beam observations of the GBT. Because they derive from filled aperture observations they are sensitive to, and include radiation from, HI of low surface brightness. They are of moderate integrated flux, 30 - 50 Jy km/s. The fluxes have been corrected for atmospheric extinction, and are on the flux scale of Ott *et al* (1994). For reference, Table 5 lists the optical and HI diameters. The HI diameters for UGC 4165 and UGC 10445 have been estimated by D.E.H. from the maps in the WHISP survey. The entries in Table 5 are as follows:

- Column 1: Galaxy identifying number, as in Table 1.
- Column 2: Optical diameter D_{25} , from RC3, in arcmin
- Column 3: HI diameter at $1 M_{\odot}/\text{pc}^2$.
- Column 4: Beam coupling factor for the 43 m telescope, f_{43m}^{BC}
- Column 5: Beam coupling factor for the GBT, f_{GBT}^{BC}
- Column 6: Ratio of the HI flux density observed with the 43 m to that observed with the GBT.
- Column 7: Predicted ratio of the beam corrected flux densities $S_{43m}^{corr}/S_{GBT}^{corr}$
- Column 8: Flux ratio index, FRI, as given by equation 5.
- Column 9: Observed 43 m HI flux density S_{43m}^{obs} , in Jy km s⁻¹.
- Column 10: Corrected 43 m HI flux density S_{43m}^{corr} , in Jy km s⁻¹.

4. Conclusions

We conclude that for $\sim 75\%$ of the galaxies in the sample the correction to the observed flux, as given in Equation 4, that is required to account for the coupling of the antenna beam to the actual distribution of HI is a good approximation, and the application of this factor will result in an estimate of the total HI line flux which has a statistical uncertainty of 5%.

The success of the model tells us that very diffuse and extended HI gas does not contribute significantly to the total HI mass in a galaxy; the reservoir of outer diffuse gas is, in the vast majority of objects, quite modest. For 88 objects in the sample, the difference between the observed and predicted flux densities is less than 10% of the total flux; for 77 of the galaxies the difference is less than 5%. In terms of the mass of HI, the latter limit differs from galaxy to galaxy; the median is $1.5 \times 10^8 M_\odot$. The surface density corresponding to the mass limit depends on the assumption of the distribution of the material. The strictest lower limit is given by assuming that the extended HI fills the beam of the 43 m. With this assumption the surface density of the putative material is of order $2 \times 10^{-2} M_\odot/\text{pc}^2$.

Even for the extensive galaxies of Table 3, the excess hydrogen over that implied by our simple HI disk model is not large. The seven systems without known companions have an average excess of only 21% in comparison with the model. Thus, our sample has demonstrated that nominally isolated galaxies do not commonly have very extended regions of low HI surface brightness.

In our sample, approximately 10% of the galaxies are more extended than described by the model, and approximately 10% have a hydrogen distribution which is more centrally condensed than anticipated. It has not been possible to identify, a priori, the galaxies for which the model failed. For example, the presence of either an extensive structure or a centrally-condensed structure does not depend upon the morphological class, the optical luminosity, or the HI mass. Thus the application of the beam correction to a sample of galaxies will inevitably introduce errors in the correction of greater than ten percent in the estimate of the total flux, for approximately 20% of the galaxies.

That the interstellar neutral hydrogen in a galaxy extends beyond its optical bounds (e.g. D_{25}) is well established and long recognized. Extreme examples of this difference, factors of 3 to 5, have also been identified. However, little notice has been taken of the opposite geometry where the HI extent is comparable to D_{25} . Such objects also occur frequently in the surveys of Broeils & Rhee (1997) and of Swaters *et al* (2002), but the reasons for the reduced size of the hydrogen envelope have not been explored in any detail. In particular, it would be of interest to know if the compact HI distribution now observed reflects the manner in which these objects were formed, or if it is a consequence of the subsequent evolution of the galaxies, including possible interactions with their environment. The sample discussed herein includes galaxies of a range of morphological types and found in relatively isolated regions.

The eight companions in Table 4 as well as an additional two to four that are likely present

in the overall sample can account for only a moderate fraction of the asymmetries seen in about half of HI velocity profiles (Paper I and references therein). The capture of companions may well explain the high frequency of such asymmetries. Our data cannot address this possibility but it may place a limit on the frequency of future capture episodes.

The designation of companionship is straightforward for those instances of a well separated pair of profiles or an obvious distortion of a profile edge. Less conspicuous instances will occur when the velocity range of the companion lay completely within the target galaxy profile and assignment of companionship can become ambiguous. Is the asymmetry due to a companion projected in velocity space onto the target profile? Is it a captured system, perhaps distorted over the face of the galaxy? Or is it an asymmetry caused by some other process, e.g. Bounard, *et al* (2005).

It is a pleasure to thank Chelen Johnson for her work with R.J.M. in developing the calibration process for the GBT data; Chris Springob for making many of the observations during the difficult second epoch; and Jim Braatz for solving the puzzle of the anomalous feature in the spectrum of one of the galaxies. In the investigation of companions we made frequent use of the NASA/IPAC Extragalactic Database (NED) which is operated by the Jet Propulsion Laboratory, California Institute of Technology, under contract with the National Aeronautics and Space Administration. In our analysis of maps of the HI distribution we benefited from the extensive survey of the neutral hydrogen component in spiral and irregular galaxies made with the Westerbork Synthesis Radio Telescope available at the WHISP web site <http://www.astro.rug.nl/~whisp/>. The complete sample of comparison profiles used in the present work is available at http://arcibo.tc.cornell.edu/hiarchive/gbt_140ft.php. This work has been partially supported by NSF grant AST-0307661 and by a Brinson Foundation grant to M.P.H.

REFERENCES

- Bajaja, E., Huchtmeier, W.K., & Klein, U. 1994, *A&A*, 285, 385
- Begum, A., Chengalur, J.N. & Karachentsev, I.D. 2005, *A&A*, 433, L1
- Bounard, F., Combes, F., Jog, C.J., & Puearari, I. 2005, *A&A*, 438, 507
- Braun, R., Thilker, D., & Walterbos, R.A.M. 2003, *A&A*, 406, 829
- Broeils, A.H. & Rhee, M.-H. 1997, *A&A*, 324, 877
- DuPrie, K. & Schneider, S.E. 1996, *AJ*, 112, 937
- Espada, D., Bosma, A., Verdes-Montenegro, L., Athanassoula, E., Leon, S., Sulentic, J., & Yun, M. S. 2005 *A&A*, 442, 455
- Fall, S.M. & Efstathiou, G. 1980, *MNRAS*, 193, 189

- Gentile, G., Salucci, P., Klein, U. & Granato, G.L. 2007, MNRAS, 375, 199
- Haynes, M.P., van Zee, L., Hogg, D.E., Roberts, M.S. & Maddalena, R.J. 1998, AJ, 115, 62 (Paper I)
- Hewitt, J.N., Haynes, M.P. & Giovanelli, R. 1983, AJ, 88, 272 (HHG)
- Hunter, D.A & Gallagher, J.S., III 1985, AJ, 90, 1789
- Larson, R.B., Tinsley, B.M. & Caldwell, C.N. 1980, ApJ, 237, 692
- Kornreich, D. A., Haynes, M. P., Lovelace, R. V. E., and van Zee, L. 2000 AJ, 120, 139
- Krumm, N. & Burstein, D. 1984, AJ, 89, 1319
- Masters, K.L., 2005, Ph.D. thesis (Cornell University)
- Meurerer, G.R., Carignan, C., Beaulieu, S.F. & Freeman, K.C. 1996, AJ, 111, 1551.
- Nilson, P. 1973. *Uppsala General Catalogue of Galaxies*, Acta Univ. Ups. Ser. V: A, Vol. 1, Uppsala. (UGC)
- Noordermeer, E., van der Hulst, J. M., Sancisi, R., Swaters, R. A., & van Albada, T. S. 2005 A&A, 442, 137
- Ott, M., Witzel, A., Quirrenbach, Krichbaum, T.P., Standke, K.J., Schalinski, C.I. & Hummel, C.A. 1994, A&A, 284, 331
- Quinn, P.J., Hernquist, L. & Fullagar, D.P. 1993, ApJ, 403, 74
- Shostak, G.S. 1978, A&A, 68, 321
- Shoskak, G.S. & Allen, R.J. 1980, A&A, 81,167
- Stil, J. M., and Israel, F. P. 2002, A&A, 389, 29
- Swaters, R.A., van Albada, T.S., van der Hulst, J.M. & Sancisi, R. 2002, A&A, 390, 829
- Tonry, J. *et al* 2000, ApJ, 530, 625
- de Vaucouleurs, G., de Vaucouleurs, A., Corwin, H. G., Jr., Buta, R. J., Paturel, G., & Fouqué, P. 1991, *Third Reference Catalogue of Bright Galaxies* (New York, Springer-Verlag) (RC3)
- van der Kruit, P.C. 1979, A&AS, 38, 15
- van Zee, L., Maddalena, R.J., Haynes, M.P. , Hogg, D.E. & Roberts, M.S. 1997, AJ, 113, 1638
- Vennik, J. & Richter, G.M. 1993, Astron. Nachr. 315, 245

Vorontsov-Velyaminov, B.A., Arhipova, V.P. 1968, *Morphological Catalog of Galaxies* (Moscow State University, Moscow) (**MCG**).

Warmels, R. H. 1988 *A&AS*, 72, 57

Zwicky, F., Herzog E., Kowal, C. T., Wild, P. & Karpowicz, M. 1961–68, *Catalogue of Galaxies and Clusters of Galaxies I–VI*, Cal. Inst. of Tech., Pasadena

Table 1. Target Galaxy Properties

U/AGC	Name	Coords (2000)	$D_{25} \times d_{25}$	T	V21 km s ⁻¹	Dist. Mpc	W21 km s ⁻¹	S_{43}^{obs} Jy km s ⁻¹	S_{GBT}^{obs} Jy km s ⁻¹	δV km s ⁻¹	rms mJy
(1)	(2)	(3)	(4)	(5)	(6)	(7)	(8)	(9)	(10)	(11)	(12)
231	N 100	002402.6 +162910	5.5 x 0.7	6	842	13.8	209	44.9	41.3	4.2	6.6
891	436-033	012119.1 +122442	2.3 x 1.0	9	643	11.4	115	17.82	16.50	4.2	5.6
947	N 514	012403.9 +125502	3.5 x 2.8	5	2472	38.2	249	27.9	25.6	4.2	4.5
1378	326-002	015619.2 +731657	3.4 x 2.3	1	2935	44.9	498	39.1	35.8	4.2	5.5
1736	N 864	021527.6 +060008	4.7 x 3.5	5	1562	24.8	224	103.0	80.8	4.2	8.3
420070	N 895	022136.1 -053114	3.6 x 2.6	6	2288	35.3	260	51.5	46.7	4.2	6.2
2141	N1012	023914.8 +300902	2.5 x 1.1	0	987	16.5	195	50.4	46.8	4.2	4.3
2259	524-020	024755.5 +373217	2.6 x 1.9	8	583	10.7	121	22.37	20.28	2.1	9.0
2302	389-024	024908.7 +020737	4.8 x 3.7	9	1104	18.2	54	58.0	53.0	2.1	11.9
420295	N1140	025433.6 -100144	1.7 x 0.9	10	1501	23.9	185	37.9	34.8	4.2	5.0
2455	N1156	025942.3 +251414	3.3 x 2.5	10	375	7.7	72	71.3	63.8	4.2	8.8
2463	540-021	030037.8 +401504	2.3 x 1.5	9	1901	28.9	195	15.39	15.10	4.2	3.4
430117	M-209019	031546.0 -120123	2.2 x 0.6	-1	3163	46.5	292	12.08	11.02	4.2	4.6
22447	357 G 12	031652.1 -353227	2.8 x 1.6	7	1567	24.3	132	23.55	22.4	4.2	5.1
430249	M-309041	032524.8 -161403	2.6 x 0.3	8	1873	28.5	232	28.2	21.64	4.2	4.6
2947	N1507	040427.3 -021110	3.6 x 0.9	9	863	14.1	178	42.2	39.3	4.2	4.6
440077	M-311019	041612.2 -164510	1.6 x 0.5	8	1953	28.7	172	10.10	10.04	4.2	3.9
440323	N1637	044128.0 -025129	4.0 x 3.2	5	717	11.7	182	77.8	56.2	4.2	9.4
3137	347-007	044615.5 +762506	3.5 x 0.4	3	992	15.8	232	47.8	41.7	4.2	6.1
450062	M-314017	052814.5 -160736	1.9 x 1.9	6	2173	30.8	75	16.59	16.89	2.1	7.4
3384		060137.4 +730700	1.7 x 1.7	9	1089	16.5	75	26.6	20.65	2.1	8.9
3574	285-010	065310.3 +571040	4.2 x 3.6	6	1441	21.0	144	39.8	38.8	4.2	4.8
3587	085-014	065354.9 +191757	2.8 x 0.7	3	1267	18.8	225	43.5	38.7	4.2	3.9
3647	M+912027	070450.9 +563114	1.4 x 1.0	10	1386	20.5	57	16.15	13.17	4.2	3.9
3826	286-016	072427.8 +614138	3.5 x 3.0	7	1733	25.2	53	24.5	23.55	2.1	12.9
3974	087-030	074155.1 +164811	3.1 x 3.0	10	272	8.0	71	61.4	54.0	4.2	8.0
4097	N2460	075652.3 +602057	2.5 x 1.9	1	1442	21.3	322	49.0	41.8	4.2	5.6
4165	N2500	080153.2 +504412	2.9 x 2.6	7	514	7.9	102	33.6	32.7	2.1	12.4
4173	349-016	080710.1 +800736	1.9 x 0.6	10	860	13.4	67	28.2	27.2	2.1	12.2
4284	N2541	081440.3 +490342	6.3 x 3.2	6	559	11.2	193	135.6	110.6	4.2	9.1
4325	N2552	081920.5 +500033	3.5 x 2.3	9	524	8.1	134	27.9	28.5	4.2	5.0
4393	237-001	082604.5 +455802	2.2 x 1.6	3	2124	31.6	112	22.19	22.2	4.2	4.9
4543	237-013	084321.5 +454409	3.3 x 1.9	8	1960	29.3	112	29.9	29.1	4.2	5.9
4605	N2654	084911.8 +601314	4.3 x 0.8	2	1347	20.7	393	45.0	36.0	4.2	3.5
4641	N2683	085241.6 +332510	9.3 x 2.2	3	411	6.3	428	80.9	65.6	4.2	5.0
5079	N2903	093209.6 +213003	12.6 x 6.0	4	556	7.9	371	224.9	270.4	4.2	9.2
190351	IZw18	093402.1 +551424	0.3 x 0.2	10	745	11.1	31	2.78	2.87	4.2	3.3
500001	M-126012	100235.8 -060058	2.8 x 0.3	7	662	8.7	123	19.77	20.14	4.2	3.7
5414	N3104	100357.1 +404520	3.3 x 2.2	10	603	7.7	102	25.0	24.8	4.2	6.9
500034	SEX A	101100.7 -044134	5.9 x 4.9	10	324	1.4	45	177.9	131.8	4.2	8.7
5662	N3245A	102701.2 +283821	3.3 x 0.3	3	1322	22.8	179	9.18	8.87	4.2	3.6
5786	N3310	103845.8 +533011	3.1 x 2.4	4	993	15.6	177	68.6	59.6	4.2	6.9
5789	N3319	103909.5 +414111	6.2 x 3.4	6	739	13.4	201	82.1	75.4	4.2	6.2
5829	184-006	104242.2 +342656	4.7 x 4.2	10	630	8.1	73	56.4	53.4	4.2	6.6
5878	N3365	104612.6 +014846	4.5 x 0.8	6	986	15.4	232	44.6	40.9	4.2	7.4
5873	N3359	104636.5 +631324	7.2 x 4.4	5	1014	16.1	244	185.8	135.5	4.2	8.4
6161	213-029	110649.1 +434322	2.6 x 1.2	8	756	9.1	115	26.8	24.6	4.2	5.8
6277	N3596	111506.2 +144712	4.0 x 3.8	5	1193	22.1	117	32.6	31.2	4.2	6.0
6420	N3666	112426.2 +112030	4.4 x 1.2	5	1060	16.1	257	49.2	44.6	4.2	4.0
6439	N3675	112608.0 +433515	5.9 x 3.1	3	770	9.3	407	58.2	45.5	4.2	3.7
6498	N3705	113007.6 +091636	4.9 x 2.0	2	1018	14.4	345	55.0	48.5	4.2	4.9
6644	N3810	114058.8 +112816	4.3 x 3.0	5	993	13.7	249	49.3	47.7	4.2	3.9
510149	N3887	114704.8 -165116	3.3 x 2.5	4	1208	22.5	236	46.3	43.1	4.2	7.6
6817	214-032	115052.7 +385250	4.1 x 1.5	10	243	2.6	36	46.0	35.2	4.2	5.9
6833	N3930	115145.8 +380051	3.2 x 2.4	5	919	12.0	152	28.8	27.9	4.2	5.6
6955	186-078	115830.5 +380436	5.0 x 2.6	10	905	11.7	149	32.6	30.9	4.2	4.7
6963	N4013	115832.1 +435653	5.2 x 1.0	3	834	10.4	393	35.2	30.4	4.2	3.2
7047	N4068	120402.2 +523519	3.3 x 1.7	10	210	4.3	52	37.1	35.1	4.2	2.6
7321	128-070	121733.9 +223224	5.5 x 0.4	7	408	3.7	219	43.3	39.9	4.2	4.2
7524	N4395	122548.8 +333247	13.2 x 11.0	9	319	4.0	119	284.6	175.0	4.2	8.2
7698	159-013	123254.5 +313230	6.5 x 4.5	10	331	2.6	60	38.3	35.9	4.2	8.1
7723	N4534	123405.5 +353105	2.6 x 2.1	8	802	9.1	118	63.4	59.3	4.2	6.0
7985	N4713	124957.9 +051839	2.7 x 1.7	7	652	7.0	165	55.0	51.8	4.2	9.3
530012	015-060	130431.0 -033419	3.5 x 2.6	8	1360	27.0	116	41.9	40.7	4.2	9.7
8490	N5204	132936.5 +582513	5.0 x 3.0	9	201	4.7	114	124.1	98.6	4.2	9.8

Table 1—Continued

U/AGC	Name	Coords (2000)	$D_{25} \times d_{25}$	T	V21 km s^{-1}	Dist. Mpc	W21 km s^{-1}	S_{43}^{obs} Jy km s^{-1}	S_{GBT}^{obs} Jy km s^{-1}	δV km s^{-1}	rms mJy
(1)	(2)	(3)	(4)	(5)	(6)	(7)	(8)	(9)	(10)	(11)	(12)
8651	218-034	133953.6 +404424	2.3 x 1.3	10	201	3.0	42	12.33	12.52	4.2	7.2
530352	M-135010	134537.9 -055906	1.7 x 1.2	9	1452	28.6	163	29.4	28.1	4.2	5.2
530375	N5324	135206.0 -060330	2.3 x 2.1	5	3042	53.3	212	28.8	26.7	4.2	4.0
8839	103-007	135524.8 +174741	4.0 x 2.7	10	957	11.9	95	24.4	22.72	4.2	5.9
9211	247-023	142232.5 +452258	1.7 x 1.4	10	686	8.0	100	25.5	24.7	2.1	6.8
9240	247-026	142443.8 +443129	1.8 x 1.8	10	150	2.8	44	24.4	23.96	2.1	11.7
9328	N5645	143039.6 +071629	2.4 x 1.5	7	1370	25.2	181	19.45	19.61	4.2	3.9
9436	N5701	143911.0 +052147	4.3 x 4.1	0	1505	27.6	119	62.0	37.6	4.2	5.5
9649	N5832	145745.7 +714053	3.7 x 2.2	3	447	4.1	156	38.4	35.9	4.2	8.4
550035	N5885	151504.0 -100507	3.5 x 3.1	5	2000	32.7	180	42.4	40.4	4.2	6.7
9935	N5964	153736.2 +055825	4.2 x 3.2	7	1447	24.0	189	39.7	38.1	4.2	4.7
10041	050-108	154901.3 +051119	3.0 x 1.7	8	2171	35.3	193	36.3	32.4	4.2	5.0
10288	023-026	161424.8 -001228	4.8 x 0.6	5	2044	30.4	360	38.2	34.7	4.2	4.1
10310	251-004	161618.2 +470244	2.8 x 2.2	9	716	9.4	89	19.79	19.86	4.2	6.7
560003	M-241001	161715.7 -114354	2.4 x 1.7	3	977	14.0	172	75.9	59.2	4.2	10.6
10350	N6118	162148.5 -021702	4.7 x 2.0	6	1573	23.6	343	35.0	33.5	4.2	3.6
10445	168-021	163347.6 +285904	2.8 x 1.7	6	963	13.8	146	29.7	27.9	4.2	5.1
560012	M-142004	164203.1 -050157	2.5 x 1.4	4	1565	23.5	287	62.7	54.4	4.2	7.2
10521	N6207	164303.8 +364958	3.0 x 1.3	5	852	11.8	225	30.1	30.4	4.2	3.9
10577	N6239	165005.5 +424421	2.6 x 1.1	3	923	13.1	212	53.2	46.7	4.2	6.7
10891	N6384	173224.3 +070336	6.2 x 4.1	4	1665	22.9	364	74.5	67.0	4.2	10.6
11218	N6643	181946.4 +743407	3.8 x 1.9	5	1484	19.2	329	36.6	34.7	4.2	5.2
600014	UA417	200921.4 -061713	2.5 x 1.3	9	1425	18.0	80	28.6	26.9	2.1	9.0
11604	N6951	203714.3 +660619	3.9 x 3.2	4	1424	18.0	314	38.4	31.8	4.2	9.4
11651	470-006	205715.4 +255806	3.1 x 0.8	8	1525	19.3	259	21.52	21.00	4.2	5.5
600179	I5078	210231.2 -164905	4.1 x 1.1	5	1474	19.3	259	42.3	36.5	4.2	4.6
11670	N7013	210333.5 +295350	4.0 x 1.4	0	779	10.5	325	19.42	20.38	4.2	4.3
11707	471-001	211431.6 +264404	3.6 x 1.9	8	906	12.1	188	57.9	55.0	4.2	9.2
610038	N7051	211951.2 -084659	1.3 x 1.1	1	2519	32.9	182	13.15	11.28	4.2	4.0
11914	N7217	220752.5 +312133	3.9 x 3.2	2	952	13.5	307	11.43	9.71	4.2	6.3
12082	495-007	223410.8 +325140	2.6 x 2.2	9	802	11.5	73	29.2	27.1	2.1	9.0
620140	M-157016	223635.0 -025425	2.5 x 2.0	9	1691	23.4	104	15.94	15.74	4.2	3.9
12329	N7468	230259.2 +163615	0.9 x 0.6	-5	2081	30.4	180	13.99	12.66	2.1	5.3
12343	N7479	230456.6 +121922	4.1 x 3.1	5	2381	34.7	352	43.0	36.5	4.2	4.9
12578	380-050	232422.9 -000632	1.6 x 1.1	9	2701	39.3	102	10.87	11.47	2.1	6.1

Table 2. Galaxies showing an extensive HI disk

U/AGC	T	FR Index	D_{25} (kpc)	D_{HI} (kpc)	D_{HI}/D_{25}	$\log M_{HI}$ M_{\odot}	$\log L$ L_{\odot}	$\log M_{HI}/L$
(1)	(2)	(3)	(4)	(5)	(6)	(7)	(8)	(9)
1736	5	-0.11	33.8	95.2 ^a	2.82	10.19	10.48	-0.29
430249	8	-0.26	21.8	9.74
440323	5	-0.23	13.5	9.41	9.83	-0.41
3384	9	-0.24	8.4	9.24
3647	10	-0.21	8.2	9.21	9.10	0.10
4605	2	-0.17	25.7	55.6 ^b	2.16	9.67	10.16	-0.49
6817	10	-0.18	3.1	5.2 ^c	1.70	7.88	7.69	0.19
9436	0	-0.41	34.3	89.8 ^d	2.62	10.06	10.41	-0.35
560003	3	-0.23	9.8	9.55
560012	4	-0.11	16.7	9.92
10577	3	-0.10	9.8	9.34	9.47	-0.13
610038	1	-0.15	12.6	9.53

^aEspada *et al* 2005

^bNoordermeer *et al* 2005

^cSwaters *et al* 2002

^dKornreich *et al* 2000

Table 3. Properties of galaxies showing a more concentrated HI disk

U/AGC	T	FR Index	D_{25} (kpc)	D_{HI} (kpc)	D_{HI}/D_{25}	$\log M_{HI}$ M_{\odot}	$\log L$ L_{\odot}	$\log M_{HI}/L$
(1)	(2)	(3)	(4)	(5)	(6)	(7)	(8)	(9)
2302	9	0.15	25.4	9.69	9.22	0.47
3574	6	0.12	25.5	38.5 ^a	1.51	9.64	9.68	-0.05
4325	9	0.10	8.2	11.1 ^b	1.36	8.65	9.10	-0.46
5789	6	0.15	24.1	34.6 ^c	1.44	9.57	9.99	-0.42
5829	10	0.12	11.0	14.8 ^b	1.34	8.96	8.54	0.42
6277	5	0.10	25.6	28.3 ^d	1.11	9.59	10.20	-0.61
6955	10	0.10	17.1	23.1 ^c	1.36	9.04	8.89	0.15
7698	10	0.18	4.9	3.7 ^e	0.76	7.82	7.88	-0.07
10891	4	0.13	41.1	9.99	10.67	-0.67
11670	0	0.14	12.2	16.1 ^f	1.32	8.72	9.95	-1.24

^aDEH/WHISP

^bSwaters *et al* 2002

^cBroeils & Rhee 1997

^dKornreich *et al* 2000

^eStil & Israel 2002

^fNoordermeer *et al* 2005

Table 4. Galaxies with Companions

Target			Companion							
U/AGC	Name	V_{\odot} km s^{-1}	U/AGC	Name	Position J2000	V_{\odot} km s^{-1}	θ arcmin	m_B	D_{25} r'	T
(1)	(2)	(3)	(4)	(5)	(6)	(7)	(8)	(9)	(10)	(11)
2141	N1012	987	121174		023951.8 +301618	810	10.7	17.	0.8 x 0.4	9
2259	524-020	583	2254		024721.6 +373129	578	6.7	17.	1.0 x 0.8	9
3384		1089	150271		060359.6 +730324	...	11.0	16.	0.5 x 0.3	7
3647	DDO 40	1386	160285	261-017	070359.2 +562911	1413	7.3	15.3	0.9 x 0.5	3
4097	N2460	1442	4093	I2209	075614.4 +601813	1371	5.4	14.3	1.1 x 0.9	3
10577	N6239	923	262744		165046.0 +424321	932	7.6	17.	0.6 x 0.4	9
430249	UA 71	1873	430687	M-309037	032512.1 -160951	1866	5.4	17.	1.0 x 0.4	9
560012	M-142004	1565	560170		164216.4 -050853	...	7.7	18.	0.4 x 0.2	9

Table 5. HI Line Flux Density Calibrators

U/AGC	D_{25} '	D_{HI} '	f_{43m}	f_{GBT}	FR^{obs}	FR^{exp}	FRI	S_{43}^{obs} Jy-km s ⁻¹	S_{43}^{corr} Jy-km s ⁻¹
(1)	(2)	(3)	(4)	(5)	(6)	(7)	(8)	(9)	(10)
2947	3.6	...	1.013	1.072	1.07	1.06	-0.02	42.2	42.8
4165	2.9	4.9 ^a	1.015	1.083	1.03	1.07	0.04	33.6	34.1
4543	3.3	4.8 ^b	1.016	1.088	1.03	1.07	0.04	29.9	30.3
7047	3.3	5.2 ^b	1.012	1.064	1.06	1.05	-0.01	37.1	37.5
7985	2.7	5.3 ^c	1.014	1.074	1.06	1.06	-0.00	55.0	55.7
10445	2.7	5.4 ^a	1.012	1.063	1.06	1.05	-0.01	29.7	30.0
10521	3.0	4.9 ^d	1.012	1.063	0.99	1.05	0.06	30.1	30.5
11218	3.8	4.2 ^d	1.019	1.101	1.06	1.08	0.02	36.6	37.3

^aDEH/WHISP

^bSwaters *et al* 2002

^cWarmels 1988

^dBroeils & Rhee 1997

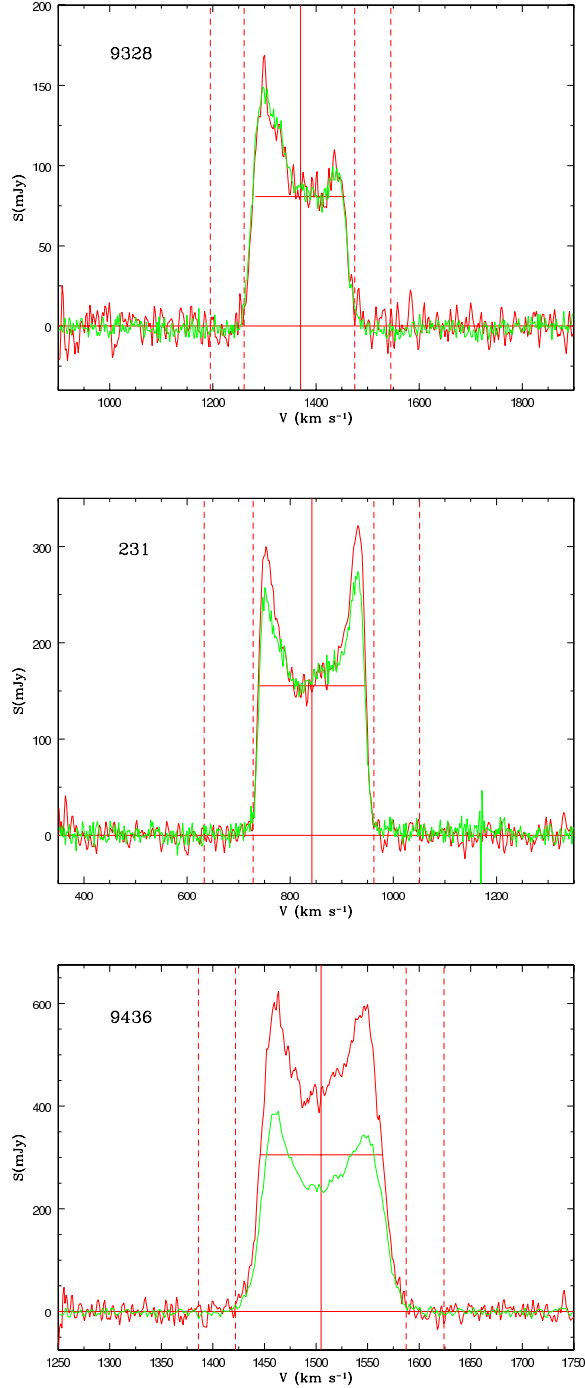


Fig. 1.— Example HI profiles obtained with the 43 m telescope (red; Paper I) and the GBT (green). The superposed number refers to the galaxy identification number given in Table 1. The solid vertical line marks the systemic HI velocity determined by the 43 m telescope observations while the solid horizontal segment shows the full width at 50% of the peak intensity as reported in Paper I. The vertical dashed lines illustrate the boundaries of the search(outer) and integration (inner) ranges used to derive integrated line flux densities as described in Section 4 of Paper I.

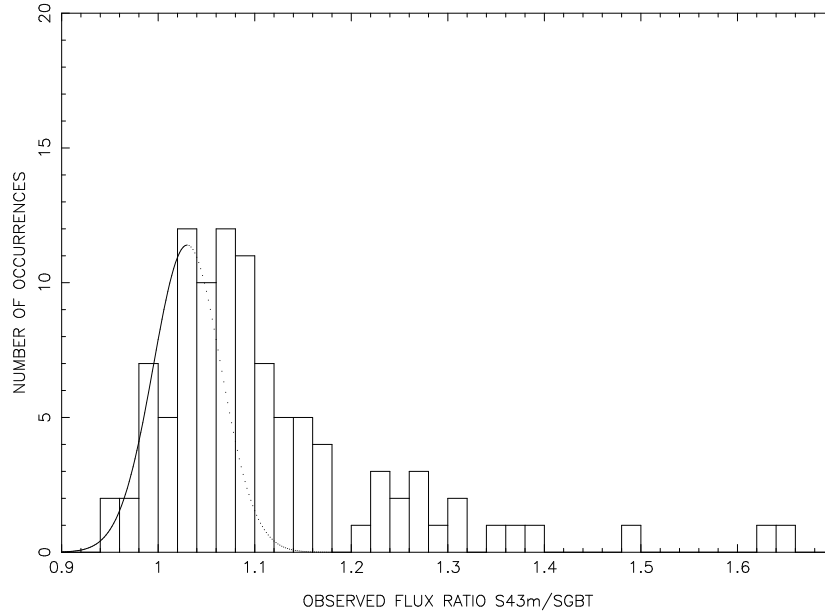


Fig. 2.— The distribution of the values of the ratio of the observed 43 m flux density to the observed GBT flux density. The Gaussian shown is centered at a ratio of 1.03 and has a standard deviation of 0.035 (see text)

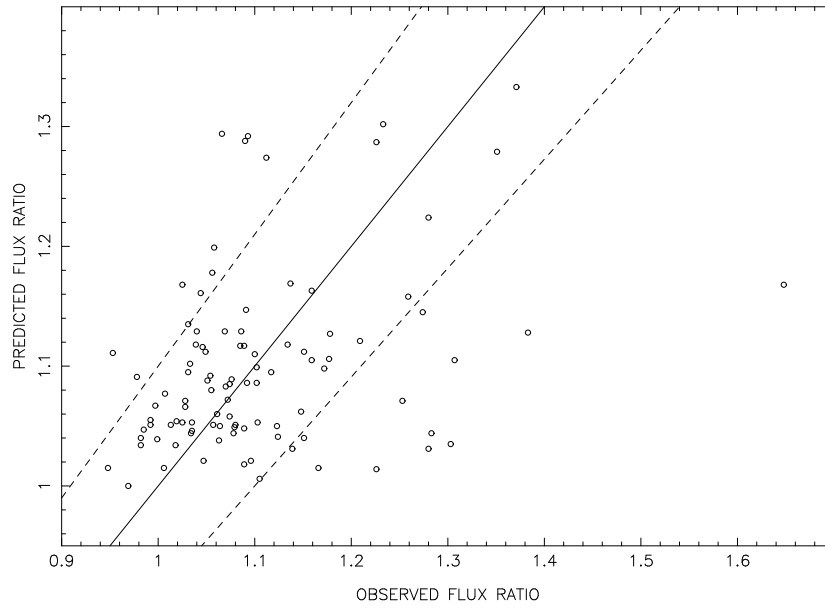


Fig. 3.— A comparison of the observed flux ratios with those predicted using a model based on the optical diameter. The solid line is the locus of equal ratios. The dashed lines delineate the regions where the observed values differ from expectation by more than 10 %. Galaxies which have centrally concentrated HI envelopes are at the upper left; galaxies having extended HI are at the lower right.

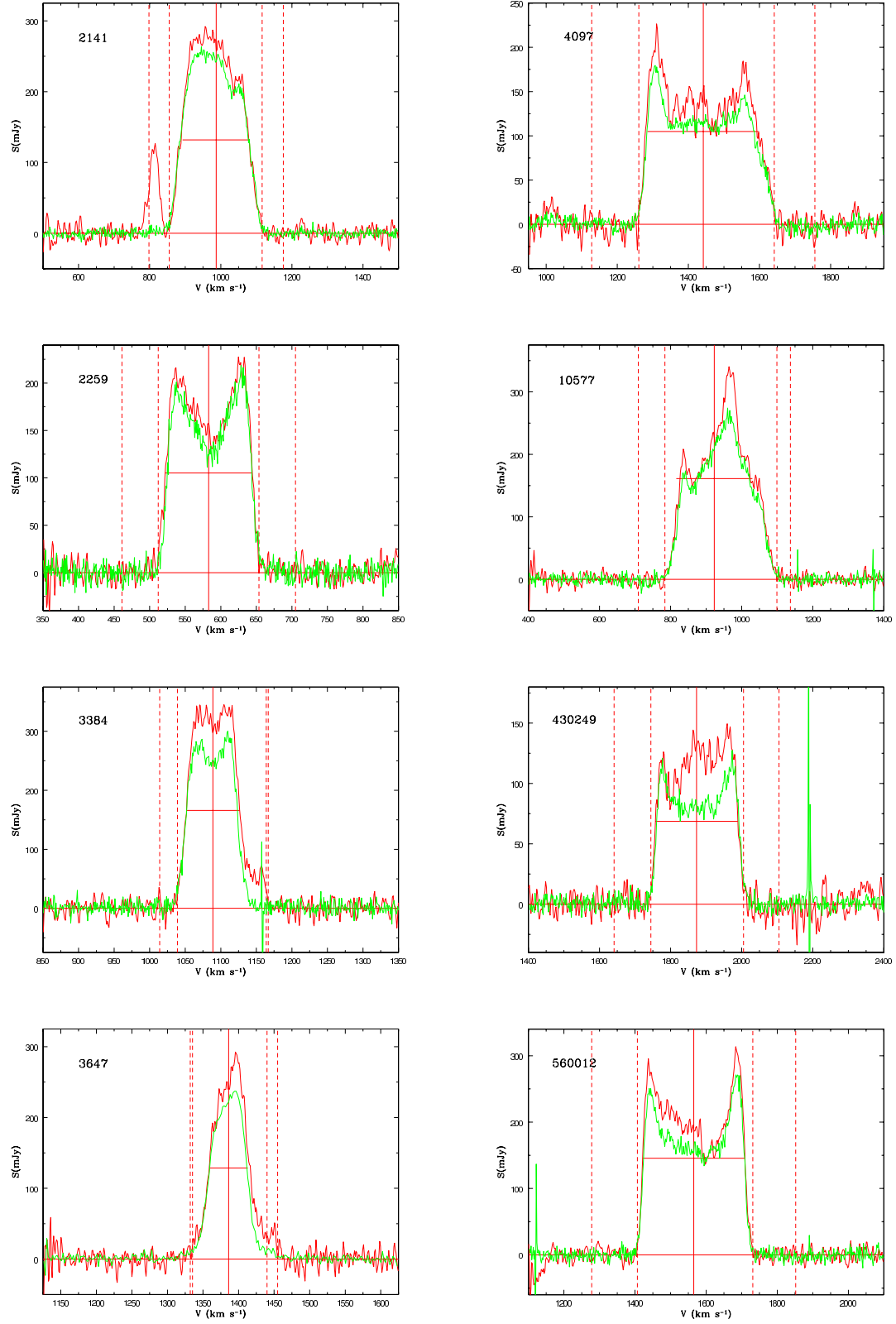


Fig. 4.— HI profiles obtained with the 43 m telescope (red) and the GBT (green) of objects with companions. Other labels and lines are as in Figure 1.

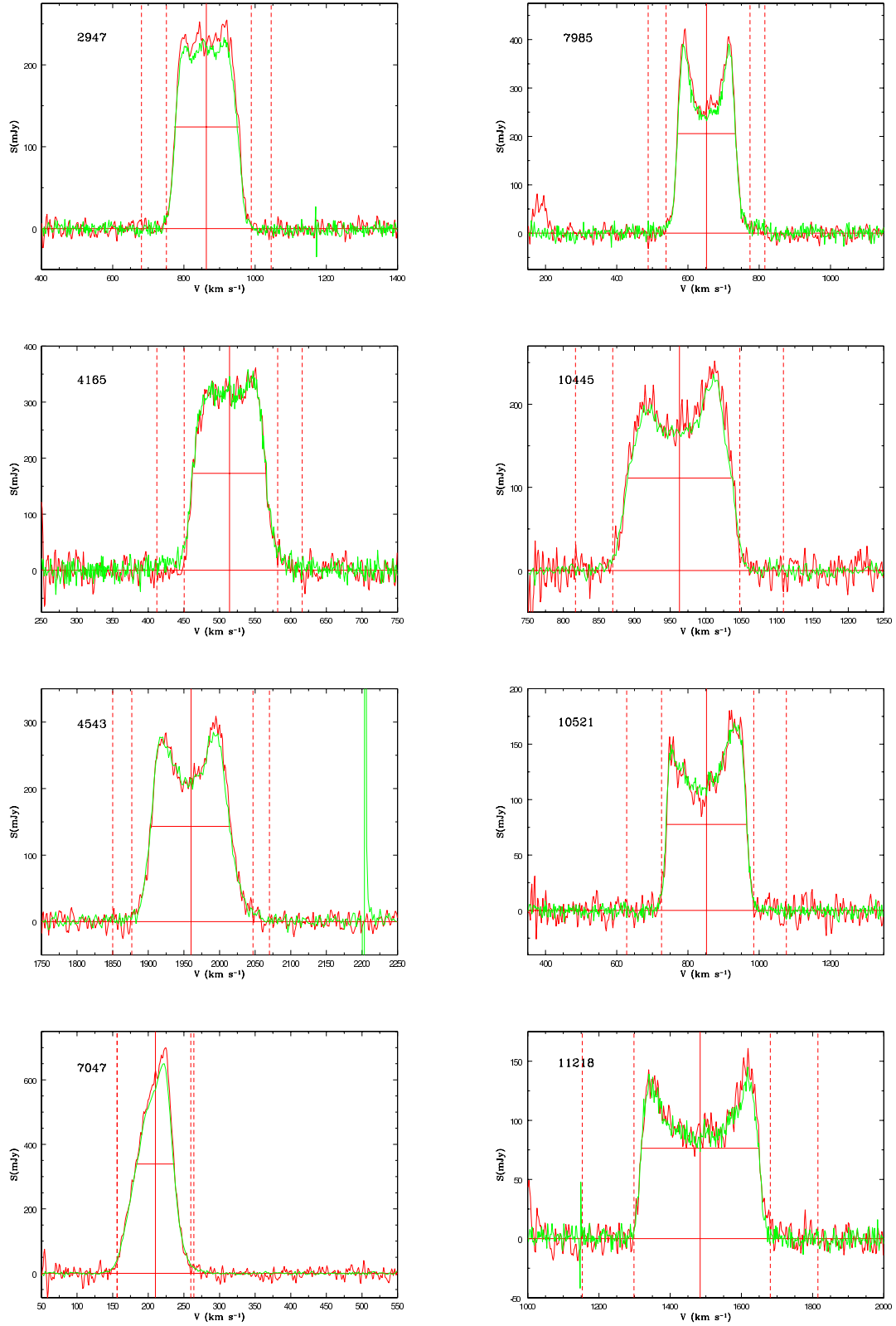


Fig. 5.— HI profiles obtained with the 43 m telescope (red) and the GBT (green) of objects included in Table 5 with small HI extent which are thus useful as HI line flux calibrators. Other labels and lines are as in Figure 1.